Medical Engineering and Physics 37 (2015) 617–622

Contents lists available at ScienceDirect

Medical Engineering and Physics

journal homepage: www.elsevier.com/locate/medengphy

Technical note

Design of an actively controlled steerable needle with tendon actuation and FBG-based shape sensing

Nick J. van de Berg*, Jenny Dankelman, John J. van den Dobbelsteen

Department of BioMechanical Engineering, Delft University of Technology, Mekelweg 2, Delft 2628CD, The Netherlands

ARTICLE INFO

Article history:
Received 20 September 2014
Revised 24 March 2015
Accepted 31 March 2015

Keywords:
Needle steering
Shape sensing
Mechanical design
Mechatronics
Automation

ABSTRACT

This work presents a new steerable needle to facilitate active steering toward predefined target locations. It focuses on mechanical aspects and design choices in relation to the observed response in a tissue phantom. Tip steering with two rotational degrees of freedom was achieved by a tendon actuated ball joint mechanism. During insertion, the flexible cannula bends as a result of asymmetric tip–tissue interaction forces. The stylet was equipped with fiber Bragg gratings to measure the needle shape and tip position during use. A PI-controller was implemented to facilitate steering to predefined targets. During the validation study, nine targets were defined at a depth of 100 mm below the gelatin surface. One was located below the insertion point, the others at a radial offset of 30 mm in each of the eight principle steering directions. Per location, six repetitions were performed. The targeting accuracy was 6.2 ± 1.4 mm (mean ± std). The steering precision was 2.6 ± 1.1 mm. The ability to steer with this new needle steering approach is presented and the mechanical characteristics are discussed for this representative subset of steering directions.

1. Introduction

Needles form a minimally invasive alternative to reach deep seated locations within the human body for diagnosis and treatment of diseased tissue. In most of these treatments, e.g. taking a liver biopsy or thermally ablating malignant structures by means of radio frequency ablation, an accurate tip placement is of importance. The operator often works with visual feedback from computed tomography (CT) or ultrasound (US) devices. Nevertheless, the risk of needle misplacement tends to increase with target depth. Placement errors can arise from human errors, imaging limitations, and needle–tissue interactions [1]. While operating flexible needles, the compensation of discovered errors can be difficult and unintuitive [2]. As placement errors become too large, needles are often completely retracted and inserted anew.

1.1. Background

The development of steerable needles is motivated by the desire to facilitate correct placements. In addition, curved paths allow targets to be reached that were formerly inaccessible. As an example, Fig. 1 presents the anatomical location of the liver with respect to surrounding structures. In particular the ribcage [3], and occasionally the lower parts of the lungs can complicate needle access.

For objective validation and comparison of steerable needles, experimental repeatability is required with a stable support, a constant insertion speed [4], an equal environment, and equal control actions. This may be obtained using computer- or robot assistance.

1.2. Related work

In the past decades, several needle steering techniques have been investigated and discussed. DiMaio and Salcudean [5] described base manipulation of unmodified clinical needles. Other passive needle steering techniques include bevel tips [6], occasionally with pre-curve [7], or flexure [8] near the tip. Active steering solutions incorporate combinations of pre-curved concentric stylets and cannulas that can translate and rotate with respect to each other [9–11]. The use of multiple interlocked segments that can individually translate resulted in an actively variable bevel [12,13]. In general, both the optimal control of passive needles and the optimal design of active needles are on-going research fields. In terms of mechanical design, passive needles are much simpler and cheaper. In terms of control robustness, active needles are potentially more adaptive to varying environmental conditions.

The key concern has been the acquisition of kinematic knowledge on non-holonomic steering constraints. Recent research focus is shifting toward practical applicability, covering the inclusion of planning

* Corresponding author. Tel.: +31 15 2782054.
E-mail address: N.J.P.vandeberg@tudelft.nl (N.J. van de Berg).

http://dx.doi.org/10.1016/j.medengphy.2015.03.016
1350-4533/

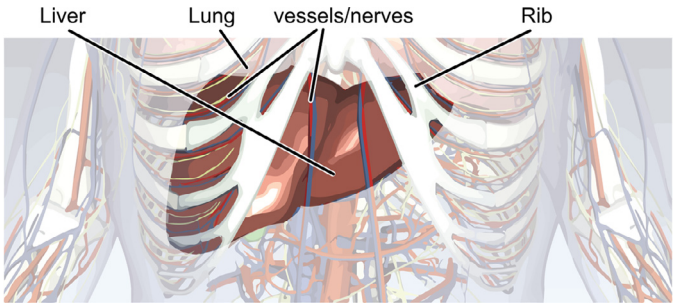

Fig. 1. Human anatomy: illustration of the liver, covered by regions of the ribcage and in variable amounts by the lungs. Image adapted from The Biodigital Human.

uncertainties with respect to tissue variability [14], the consideration of torsional friction [15], and the reduction of model dependencies on a-priori information [16].

1.2.1. Performance metrics

Many needle steering studies have focused on the evaluation of path planners (for a review see [1]). Control actions for these methods are determined a priori and occasionally updated intra-operatively, e.g. [17,18]. Planning paths requires (inverse) kinematic expressions for needle motion. To assess the error build-up of a steering task, some form of trajectory error [19] or end-point error [16,20] is generally reported. For this, position information is acquired by various sensors, such as cameras [21,22], electromagnetic sensors [12], ultrasound probes [23], fluoroscopic X-ray [24], and fiber Bragg gratings (FBGs) [25–27].

Typically, kinematic expressions rely on shape assumptions, such as a piecewise constant radius of curvature [28]. Therefore, radius of curvature is an often used metric to characterize kinematic models [7,29–31]. The validity of constant radius path approximations, however, has in the past been debated for certain needle–environment combinations [6,32].

For needles that require rotations to select a steering plane, torsion may affect target reachability and is typically assessed [33,34]. In analogy, for needles that do not rotate, a representative subset of steering planes should be selected to investigate directional symmetry in actuation. Kinematic responses may differ due to various imperfections in the designing, machining and assembling process. In a study of Burrows et al. [35], the eight principal steering directions (every 45°) of an adaptable bevel tip needle were evaluated. Kinematic differences were found and attributed to variations of the needle's flexural rigidity for different tip configurations.

1.3. Aim

This article presents a novel actively steered needle and focuses on its mechanical design. The needle is composed of a flexible cannula and has a conical tip that can rotate with two orthogonal degrees of freedom. During insertion, the needle will deflect as a result of asymmetric reaction forces at the needle–tissue interface. In order to track the needle shape and tip location, FBGs have been integrated in the stylet. This stylet can be withdrawn after placement, leaving the cannula as working channel. The characteristics of the shape-sensing stylet have been analyzed for various configurations and deformations [26,36]. Since the insertion stroke is considered constant, 2D targeting errors (top view) are presented for the eight principal steering directions. To the author's knowledge, this is the first study to combine an active needle steering method with FBG-based shape feedback. The obtained shape information can ultimately provide an overlay on static or dynamic visual information from CT or ultrasound devices, in order to continuously update the tip position with respect to the target.

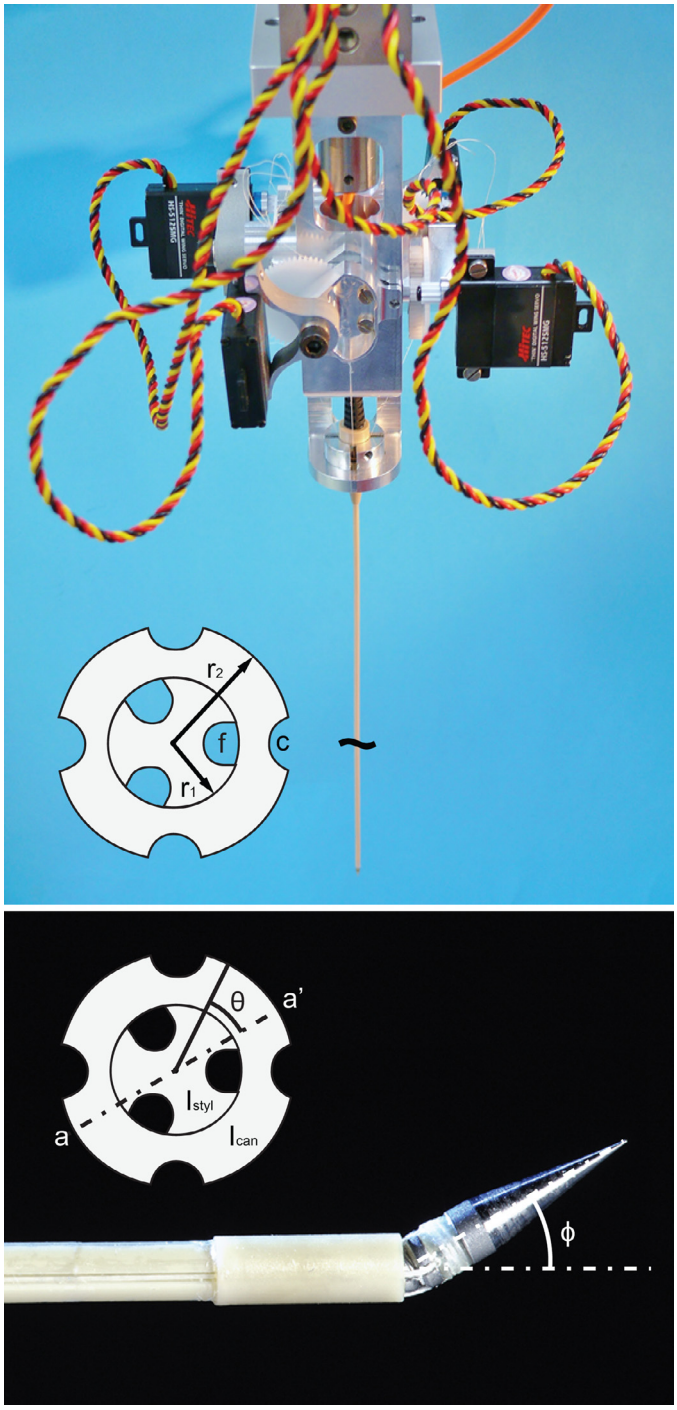

Fig. 2. The tendon-driven needle consists of a stylet with radius r_1 and grooves for optical fibers (f), and a cannula with radius r_2 and grooves for the actuation cables (c). Steering is achieved by four servo motors located at the needle base. This results in tip rotations with a magnitude (ϕ) up to 20° in any orientation (θ).

2. Methods

2.1. Mechanical needle design

The steerable needle used in this study is shown in Fig. 2. It is composed of a flexible cannula, a retractable sensorized stylet and a 5 mm long conical tip (apex angle of 20°) placed on top of a ball joint. The ball joint is tendon driven and actuated by 4 rotary servo motors (Hitec HS-5125 MG) working in complementary pairs. By alteration of the servo positions, the needle tip can rotate with 2 orthogonal

rotational degrees of freedom (DOF). The combined effect of servo motor actuations allows for steering in any direction (tip orientation θ). The motors are rigidly fixed to a linear stage (Festo EGSL-BS-55-250-12.7P) that realizes the insertion, providing a 3 DOF system.

The 170 mm long needle consists of a stainless steel stylet, 0.5 mm radius (r_1), and three grooves for optical fibers (f). The PEEK plastic (IDEX® Health & Science) cannula, 0.9 mm radius (r_2), contains four grooves for steering cables (c). Finally, a layer of PET plastic heat-shrink tubing (Vention Medical®) keeps the grooves clean and the cables in place. The outer needle radius is approximately 1 mm. This resembles a 14–15 G needle, which is regularly used during liver biopsies [37].

Four actuation cables are fixed at the tip, run over the ball joint, along the cannula and exit the needle hub. Each cable was fixed to a rack that connects to one of the servo motors. Before this connection was made, linear tension springs provided a pretension of approximately 1 N. After the connection, the springs serve to reduce gear play. The gear transmission was chosen in such a way that the linear translations of the racks allow tip rotations (steering magnitude ϕ) of approximately 20°.

The degree of bending under influence of a steered tip depends on the force interaction at the tip and the flexural rigidity of the needle. An approximation of the shaft's flexural rigidity was obtained from the stylet (styl) and cannula (can) geometry:

$$[E \cdot I]_{Needle} = E_{SS} \cdot I_{styl} + E_{PEEK} \cdot I_{can} \tag{1}$$

where E is the Young's modulus (E_{SS} = 200 GPa, E_{PEEK} = 3.4 GPa), and I the second moment of area. For a circular and annulus shaped cross-sections, this becomes:

$$[E \cdot I]_{Needle} = \frac{E_{SS} \cdot \pi}{4} \cdot r_1^4 + \frac{E_{PEEK} \cdot \pi}{4} \cdot \left(r_2^4 - r_1^4\right) \tag{2}$$

An extended version of this formula with grooves in the needle stylet and cannula would somewhat decrease the associative second moments of area, resulting in a flexural rigidity of 7.8×10^{-3} N m^2. Using the steerable needle with a dummy stylet, some small weights, and the cantilever beam formula, a validation experiment provided a value of 8.2×10^{-3} N m^2. This approaches a conventional, fine 20 G stainless steel needle (6.7×10^{-3} N m^2). In the case of a constant curvature approximation, this value would relate the curvature, κ, to the applied bending moment, M:

$$\kappa = M/[E \cdot I]_{Needle} \tag{3}$$

With regard to rotational symmetry of bending, the Huygens–Steiner theorem shows that the second moment of area remains unaffected by steering orientation if the summed effect of the grooves in the cannula and stylet is rotationally symmetric (independent of θ). This effect is described by the grooves' squared distances (r) to the neutral line and the cross-sectional areas (A), according to:

$$I(\theta) = I_0 - \sum (A \cdot r(\theta)^2) = c \tag{4}$$

Here, I_0 is the second moment of area of a grooveless needle. It can be shown that, both in case of a circle with three rotationally symmetric grooves, and in case of an annulus with four rotationally symmetric grooves, the second moment of area remains constant. Hence, the steering orientation should not affect bending of the individual parts, nor that of the needle in total.

2.1.1. Cannula shape reconstruction

The needle shape is reconstructed on the basis of strain measurements by three optical fibers. In each fiber, there are 4 FBGs (HI-780 (acrylate recoating), Corning Incorporated, Corning, USA). They are located at [20 60 100 140] mm from the cannula hub. Wavelengths reflected by the FBGs are read-out by a Deminsys interrogator (Technobis group, Alkmaar, The Netherlands). The sensors have been calibrated under constant curvature and the needle shape is extrapolated from the unfiltered fiber strain data. The approach, used methodology and sensing precision are the same as in our previous study [26]. The precision of the estimated tip location, extrapolated from this sequence of strain measurements, is approximately 1 mm. A more detailed analysis of errors due to variations in needle configuration and deformation can be found in [26] and [36].

2.1.2. Control of the needle tip

The linear stage has an integrated PID controller and operates at a constant speed of 5 mm/s to a depth of 100 mm. Tip steering is regulated by means of the servo motors and is possible for as long as the stage stroke lasts. A digital PI-controller is implemented. The reference variable is the top-view (x–y) tip position error with respect to a pre-set target. The controller output for the x-direction (same for y) is:

$$u_x(t) = K_p e_x(t) + K_i \int_0^t e_x(\tau) d\tau \tag{5}$$

Here, K_p (=0.1) is the proportional gain, K_i (=0.05) the integral gain, and e_x the error between the measured tip position and the target ($x - x_t$). An iteration consists of 4 steps: (1) the read-out of new sensor data, (2) the shape reconstruction and visualization, (3) the tip error and controller output determination, and (4) the servo actuation. The median iteration time was ~0.1 s. This is considered sufficient for the slow moving needle. Tuning of the steering response was done in an iterative manner in the selected test environment based on the ability to approximate targets with a single smooth curve. In addition, FBG measurements are used to sense first tissue contact. For this, a radial tip displacement threshold of 0.5 mm from the calibrated initial shape was used. The control gains were kept small, but nonzero, up to this event to ensure a near straight tip during puncturing. After this, the PI gains were gradually built up within 50 iterations.

2.2. Experimental setup

Experiments were performed in a 15 m% porcine gelatin–water mixture (Dr. Oetker, The Netherlands). In terms of stiffness, this should be within the order of magnitude of 10 kPa, which we consider clinically relevant for simulating liver structures. The mixture was prepared at 70 °C, congealed and stored at 2 °C, and retrieved just before the experiments. The same phantom was used to assess control parameters and to perform targeting experiments. To get rid of prior paths, a single reheat-cool cycle was needed. Fig. 3 shows the phantom, the tip-steered needle and a guiding block (trocar) for support.

2.3. Experimental design

The target depth was kept constant (z = 100 mm). In total, 9 different targets with respect to the needle insertion point were defined. This includes the [x,y] = [0,0] coordinate, and the eight principal steering directions, with θ at every 45°, using a radial offset of 30 mm with respect to [0,0]. The distance between insertion points was at least 10 mm to avoid path crossing. For each of the targets, 6 puncture repetitions were performed. Each puncture consists of a constant speed stage stroke, where re-targeting was not allowed. The tip coordinates were tracked and recorded.

2.4. Analysis

The tip position was determined at the end of the linear stage stroke. Position data was filtered with a 3rd order low-pass Butterworth filter, using a cut-off frequency of 0.5 Hz. The steering accuracy per target (mean ± standard deviation) was determined by the in-plane error between the tip and target (x_t, y_t). The steering precision with respect to the average position reached ($\bar{x}$, $\bar{y}$) is also shown,

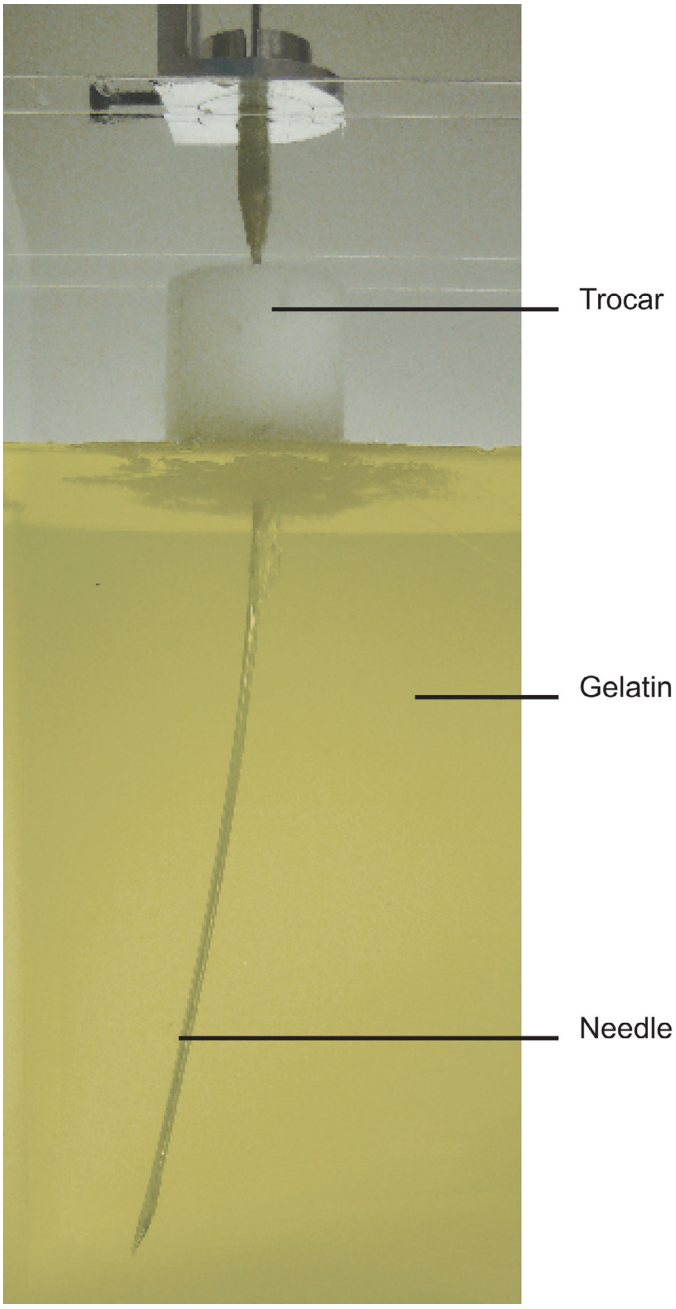

Fig. 3. Image capture of needle steering in gelatin. A trocar was used to prevent buckling at the needle base.

which indicates the repeatability of puncture events, irrespective of systematic effects on the tip placement:

$$\text{Accuracy} = \frac{\sum_1^n \sqrt{(x - x_t)^2 + (y - y_t)^2}}{n} \tag{6}$$

$$\text{Precision} = \frac{\sum_1^n \sqrt{(x - \bar{x})^2 + (y - \bar{y})^2}}{n} \tag{7}$$

3. Results

The main goal of this study is to analyze the mechanics of this steering technique and to understand its systematic behavior, irrespective of the exact type of controller that is used. A top view (x–y plane) of all needle tip trajectories is shown in Fig. 4. Visible effects in this graph can be attributed to both the mechanical and the control design. Overall, a definite steering behavior in gelatin was witnessed. The targeting accuracy was 6.2 ± 1.4 mm. The precision was 2.6 ± 1.1 mm.

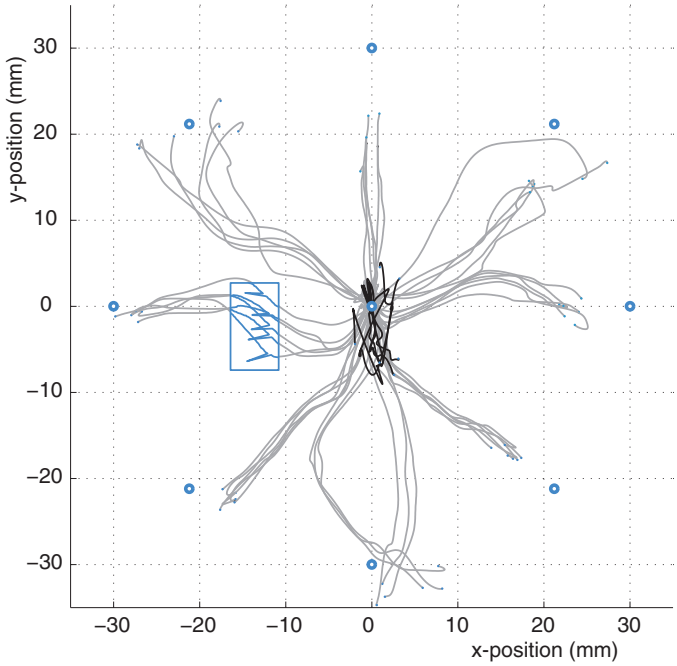

Fig. 4. Top view (x–y plane) of needle tip trajectories. Nine target locations were selected for controlled steering experiments. Data within the rectangle are unfiltered.

The initial tip heading was not always in line with the target, as control actions were deliberately built up at the start. As the gain increased, for some trajectories this led to slight s-curves in top view. Other steering conditions showed an early bifurcation in their trajectories. This happened for instance at $[x,y] = [0,0]$ and $[x,y] = [0,-30]$. These effects had a large impact on both the mean and spread of the reported precision. For some tip orientations, the set gain was sufficient, whereas for others it was not, e.g. $[x,y] = [0,30]$.

On rare occasions, strain sensing inaccuracies were witnessed that were not present in reality. Since these inaccuracies had a cumulative effect during shape reconstruction, they showed up as discontinuities in the presented tip position. Within the rectangular box in Fig. 4, unfiltered tip position data is shown, including some of these effects. Typically, these reconstruction errors lasted a single iteration and occurred in the same insertion phase for different trials. Here, the cannula loading conditions were presumed comparable.

4. Discussion

It has been acknowledged that, although a great deal of progress in needle modeling and control has been achieved, comparatively little attention has been paid to needle design [8]. This article presents a novel, active tip-steered needle and in this, purely focuses on describing the underlying working mechanisms. The needle operates by means of an actively controlled ball joint near the tip. This allows tip rotations with two orthogonal degrees of freedom. No cannula rotations are required to change the steering direction. FBG-based shape sensing was integrated in the needle stylet and used to construct a closed loop PI controller for reducing the target error. The shape-stylet is removable after placement. Steering experiments were performed in gelatin and analyzed. This provides a solid basis for future optimization of this steering technique.

In terms of experimental results, some systematic effects in target reachability were noted for different steering directions. In theory,

these differences can be explained by the interaction mechanics. Two known contributing factors were the slight needle pre-curvature and the position tolerance of the tendon fixations. The PEEK tubing was not perfectly straight (radius of curvature in the order of 10 m), which may have led to base manipulation effects. The second effect is, however, presumed more dominant. The tendon fixations determine the transmission between the linear displacement and the tip rotation. The steering response is very sensitive to inaccuracies here.

In contrast to typical non-steered insertions, steerable needles may attain more complex, multi-curved shapes. Whether or not robot assistance or shared control of steerable needles will at some point be superior to manual use in clinical practice, is left open. Likely, this will rely on the achievable degree of targeting robustness in highly variable and poorly known environments. The prospect of needle steering will rely on the development of mechanically robust needle designs, suitable control methods, and high quality system feedback.

For feedback on the needle tip position, our study used FBGs with a precision of ~1 mm. This precision may, however, decrease with needle shape complexity. The used strain interpolation function is well able to capture intermediate values, but its validity decreases with shape complexity. Dependent on the clinical task, more FBGs per optical fiber may be desired. However, for typical liver interventions, tracking of single bends should be sufficient.

4.1. Mechanical considerations

It was found that the tension levels in the tendons affect not just the relation between tip orientation (θ) and magnitude (ϕ), but also the friction within the ball joint. Above a certain normal force threshold, stick-slip phenomena prevent joint rotations altogether, allowing for direct cannula bending upon actuation. Depending on the envisioned clinical application, this may be used to compensate for the cannula pre-curvature. Moreover, this balance may provide an adaptable stiffness mechanism, e.g. servo-controlled setting of tension levels, which may be used to navigate under various environmental conditions.

With a flexural rigidity of approximately 8×10^{-3} N m^2, our needle is comparable to conventional 20 G fine needles used in every day practice. Comparable needles are also used during base manipulation needle steering [23]. Although multiple curves are possible, our needle is considerably stiffer than the needles used during passive needle steering studies. Bevel tip steering, for instance, is typically done with 0.36–0.7 mm diameter flexible wire [7,28,29]. These needles would have a flexural rigidity that is one or two orders of magnitude smaller than a 20 G needle. The effect of bending stiffness on the steering response and on robust control would be an interesting follow-up study.

4.2. Control considerations

A generic PI controller with equal gains for all tip orientations is used in this study. More complex controllers will likely benefit the placement accuracy, but simultaneously complicate the mechanical assessment. The controller used includes the current x- and y-error measurements with respect to the set target. This controller is naïve in the sense that it is not aware of remaining stroke length (z-direction) and does not include this in tip angle computations. A customized kinematics or mechanics-based predictive model may be used in the future. An overview of some of the available path planning options is provided by Gao et al. [1].

With regard to the reported single iteration tracking inaccuracies in the FBG-based shape feedback, it should be noted that the overall effect on steering is small. Due to the low insertion speed, the vertical tip displacement in one iteration is minimal. In addition, needle steering is a non-holonomic process in which lateral tip-motions are confined. Nevertheless, these artifacts should be removed, e.g. by applying burst mode data sampling.

Similar to the suggestion of making the mechanical stiffness of a needle variable, an adaptable control strategy based on the navigation medium may be desired. Both methods would require some mechanical information on the tissue structures ahead, which may be obtained through pre-operative scans or perhaps, in the future, through actual on-site measurements.

5. Conclusion

This study presents the mechanical characteristics of a new needle steering method. Closed loop steering to predefined targets with an active tip-steered needle under FBG-based shape feedback was evaluated. With this needle design and the most basic control method, a targeting accuracy of 6.2 ± 1.4 mm, and a precision of 2.6 ± 1.1 mm was reached. Fundamental research in needle–tissue interactions is ongoing and should improve both the mechanical design and the control approach.

Conflict of interest

None.

Acknowledgment

This work was supported by the Stichting voor Technische Wetenschappen [nr. 12159]; and the Austrian Center for Medical Innovation and Technology.

References

[1] Gao DD, Lei Y, Zheng HJ. Needle steering for robot-assisted insertion into soft tissue: a survey. Chin J Mech Eng 2012;25:629–38.
[2] Asadian A, Kermani MR, Patel RV. Robot-assisted needle steering using a control theoretic approach. J Intell Robot Syst 2011;62:397–418.
[3] Wolf DC. Evaluation of the size, shape, and consistency of the liver. In: Walker HK, Hall WD, Hurst JW, editors. Clinical methods: the history. 3rd ed. Boston: Physical, and Laboratory Examinations; 1990.
[4] Podder TK, Sherman J, Clark DP, Messing EM, Rubens DJ, Strang JG, et al. Evaluation of robotic needle insertion in conjunction with in vivo manual insertion in the operating room. Proc IEEE Robot and Human Interact Commun (RO-MAN) 2005:66–72.
[5] DiMaio SP, Salcudean SE. Needle steering and model-based trajectory planning. Proc Med Image Comput Comput Assist Interv (MICCAI) 2003;2878:33–40.
[6] Alterovitz R, Goldberg K, Okamura A. Planning for steerable bevel-tip needle insertion through 2D soft tissue with obstacles. Proc IEEE Robot Autom (ICRA) 2005;1–4:1640–5.
[7] Wedlick TR, Okamura AM. Characterization of pre-curved needles for steering in tissue. Proc IEEE Eng Med Biol Soc (EMBS) 2009:1200–3.
[8] Swaney PJ, Burgner J, Gilbert HB, Webster RJ, 3rd. A flexure-based steerable needle: high curvature with reduced tissue damage. IEEE Trans Biomed Eng 2013;60:906–9.
[9] Okazawa S, Ebrahimi R, Chuang J, Salcudean SE, Rohling R. Hand-held steerable needle device. Trans Mechatron 2005;10:285–96.
[10] Sears P, Dupont P. A steerable needle technology using curved concentric tubes. Proc IEEE RSJ Intell Robot Syst (IROS) 2006:2850–6.
[11] Webster RJ. Towards active cannulas: miniature snake-like surgical robots. Proc IEEE RSJ Intell Robot Syst (IROS) 2006:2857–63.
[12] Ko SY, Davies BL, Rodriguez Y, Baena F. Two-dimensional needle steering with a "programmable bevel" inspired by nature: modeling preliminaries. Proc IEEE RSJ Intell Robot Syst (IROS) 2010:2319–24.
[13] Oldfield MJ, Burrows C, Kerl J, Frasson L, Parittotokkaporn T, Beyrau F, et al. Highly resolved strain imaging during needle insertion: results with a novel biologically inspired device. J Mech Behav Biomed 2014;30:50–60.
[14] Alterovitz R, Branicky M, Goldberg K. Motion planning under uncertainty for image-guided medical needle steering. Int J Robot Res 2008;27:1361–74.
[15] Reed KB, Okamura AM, Cowan NJ. Modeling and control of needles with torsional friction. IEEE Trans Biomed Eng 2009;56:2905–16.
[16] Rucker DC, Das J, Gilbert HB, Swaney PJ, Miga MI, Sarkar N, et al. Sliding mode control of steerable needles. IEEE Trans Robot 2013;29:1289–99.
[17] Reed KB, Kallem V, Alterovitz R, Goldberg K, Okamura AM, Cowan NJ. Integrated planning and image-guided control for planar needle steering. Proc IEEE RAS EMBS Biomed Robot Biomechatron (BioRob) 2008:819–24.
[18] Minhas D, Engh JA, Riviere CN. Testing of neurosurgical needle steering via duty-cycled spinning in brain tissue in vitro. Proc IEEE Eng Med Biol Soc (EMBS) 2009:258–61.

[19] Glozman D, Shoham M. Image-guided robotic flexible needle steering. IEEE Trans Robot 2007;23:459–67.
[20] Romano JM, Webster RJ, Okamura AM. Teleoperation of steerable needles. Proc IEEE Robot Autom (ICRA) 2007;1–10:934–9.
[21] DiMaio SP, Salcudean SE. Needle steering and motion planning in soft tissues. IEEE Trans Biomed Eng 2005;52:965–74.
[22] Webster RJ, Memisevic J, Okamura AM. Design considerations for robotic needle steering. Proc IEEE Robot Autom (ICRA) 2005;1–4:3588–94.
[23] Neubach Z, Shoham M. Ultrasound-guided robot for flexible needle steering. IEEE Trans Biomed Eng 2010;57:799–805.
[24] Majewicz A, Wedlick TR, Reed KB, Okamura AM. Evaluation of robotic needle steering in ex vivo tissue. Proc IEEE Robot Autom (ICRA) 2010:2068–73.
[25] Park YL, Elayaperumal S, Daniel B, Ryu SC, Shin M, Savall J, et al. Real-time estimation of 3-D needle shape and deflection for MRI-guided interventions. Trans Mechatron 2010;15:906–15.
[26] Henken K, Van Gerwen D, Dankelman J, Van Den Dobbelsteen J. Accuracy of needle position measurements using fiber Bragg gratings. Minim Invasiv Ther 2012;21:408–14.
[27] Roesthuis RJ, Kemp M, van den Dobbelsteen J, Misra S. Three-dimensional needle shape reconstruction using an array of fiber Bragg grating sensors. Trans Mechatron 2014;19:1115–26.
[28] Webster RJ, Kim JS, Cowan NJ, Chirikjian GS, Okamura AM. Nonholonomic modeling of needle steering. Int J Robot Res 2006;25:509–25.
[29] Misra S, Reed KB, Schafer BW, Ramesh KT, Okamura AM. Mechanics of flexible needles robotically steered through soft tissue. Int J Robot Res 2010;29:1640–60.
[30] Majewicz A, Marra SP, van Vledder MG, Lin M, Choti MA, Song DY, et al. Behavior of tip-steerable needles in ex vivo and in vivo tissue. IEEE Trans. Biomed Eng 2012;59:2705–15.
[31] Kallem V, Cowan NJ. Image guidance of flexible tip-steerable needles. IEEE Trans Robot 2009;25:191–6.
[32] Rucker DC, Webster RJ, Chirikjian GS, Cowan NJ. Equilibrium conformations of concentric-tube continuum robots. Int J Robot Res 2010;29:1263–80.
[33] Reed KB, Okamura AM, Cowan NJ. Controlling a robotically steered needle in the presence of torsional friction. Proc IEEE Robot Autom (ICRA) 2009:3476–81.
[34] Swensen J, Lin M, Okamura A, Cowan N. Torsional dynamics of steerable needles: modeling and fluoroscopic guidance. IEEE Trans Biomed Eng 2014;61:2707–17.
[35] Burrows C, Secoli R, Rodriguez Y, Baena F. Experimental characterization of a biologically inspired 3D steering needle. Proc Control Autom Syst (ICCAS) 2013:1252–7.
[36] Henken KR, Dankelman J, van den Dobbelsteen JJ, Cheng LK, van der Heiden MS. Error analysis of FBG-based shape sensors for medical needle tracking. IEEE – ASME Trans Mechatronics 2014;19:1523–31.
[37] Cholongitas E, Senzolo M, Standish R, Marelli L, Quaglia A, Patch D, et al. A systematic review of the quality of liver biopsy specimens. Am J Clin Pathol 2006;125:710–21.